Catalysis Today 312 (2018) 35–43

Contents lists available at ScienceDirect

Catalysis Today

journal homepage: www.elsevier.com/locate/cattod

Understanding zeolite-catalyzed benzene methylation reactions by methanol and dimethyl ether at operating conditions from first principle microkinetic modeling and experiments

Kristof De Wispelaere[a,b,c,*], Juan S. Martínez-Espín[d,e], Max J. Hoffmann[a,b], Stian Svelle[d], Unni Olsbye[d], Thomas Bligaard[a,b]

[a] SUNCAT Center for Interface Science and Catalysis, SLAC National Accelerator Laboratory, 2575 Sand Hill Road, Menlo Park, CA, 94025, USA
[b] Department of Chemical Engineering, Stanford University, Stanford, CA, 94305, USA
[c] Center for Molecular Modeling, Ghent University, Technologiepark 903, B-9052, Ghent, Belgium
[d] Centre for Materials Science and Nanotechnology, Department of Chemistry, University of Oslo, P.O. Box 1033, Blindern, N-0315 Oslo, Norway
[e] Haldor Topsøe A/S, Haldor Topsøes Allé 1, DK-2800 Kongens Lyngby, Denmark

ARTICLE INFO

Keywords:
Zeolites
Methanol-to-hydrocarbons
Microkinetic modeling
Methylation
Methanol
Dimethyl ether

ABSTRACT

In methanol-to-hydrocarbon chemistry, methanol and dimethyl ether (DME) can act as methylating agents. Therefore, we focus on the different reactivity of methanol and DME towards benzene methylation in H-ZSM-5 at operating conditions by combining first principles microkinetic modeling and experiments. Methylation reactions are known to follow either a concerted reaction path or a stepwise mechanism going through a framework-bound methoxide. By constructing a DFT based microkinetic model including the concerted and stepwise reactions, product formation rates can be calculated at conditions that closely mimic the experimentally applied conditions. Trends in measured rates are relatively well reproduced by our DFT based microkinetic model. We find that benzene methylation with DME is faster than with methanol but the difference decreases with increasing temperature. At low temperatures, the concerted mechanism dominates, however at higher temperatures and low pressures the mechanism shifts to the stepwise pathway. This transition occurs at lower temperatures for methanol than for DME, resulting in smaller reactivity differences between methanol and DME at high temperature. Our theory-experiment approach shows that the widely assumed rate law with zeroth and first order in oxygenate and hydrocarbon partial pressure is not generally applicable and depends on the applied temperature, pressure and feed composition.

1. Introduction

In industrial chemical reactions such as the methanol-to-hydrocarbons (MTH) or xylene production, zeolite-catalyzed methylation reactions are crucial reaction steps [1–3]. In recent years, many theoretical and experimental groups studied methylation reactions of alkenes and aromatics by several methylating agents to gain insight into the mechanism, kinetics and the effect of the zeolite characteristics and operating conditions [3–14]. During the early stages of the MTH reaction, a mixture of methanol (MeOH) and dimethyl ether (DME) is formed. However, MeOH-DME equilibrium is not always established because the rate of MeOH dehydration to DME is similar to the rates of methylation reactions over strong Brønsted acid sites (BAS) [15]. Hence, under MTH conditions, both MeOH and DME act as methylating agents.

It is well-known that zeolite-catalyzed methylations can occur via two distinct mechanisms (Fig. 1) [3]. In a concerted reaction step the oxygenate transfers its methyl group directly to the hydrocarbon, with the simultaneous formation of methanol or water. The stepwise mechanism goes through a framework-bound methoxide, formed by the oxygenate. For both mechanisms it is assumed that the oxygenate adsorbs first, as it can form strong hydrogen bonds with the BAS, and that the hydrocarbon co-adsorbs.

Both mechanisms are assumed to occur during zeolite-catalyzed methylation reactions and the occurrence of one or the other mechanism was found to critically depend on the zeolite topology and the applied reaction conditions [10,14,16–19]. Similar conclusions were drawn for methanol dehydration to form DME [17,20,21]. The coverage of the surface by methoxides becomes increasingly important with increasing temperature due to the entropic gain associated with

* Corresponding author at: Center for Molecular Modeling, Ghent University, Technologiepark 903, B-9052, Ghent, Belgium.
E-mail address: Kristof.dewispelaere@ugent.be (K. De Wispelaere).

https://doi.org/10.1016/j.cattod.2018.02.042
Received 29 November 2017; Received in revised form 7 February 2018; Accepted 23 February 2018
Available online 24 February 2018
0920-5861/

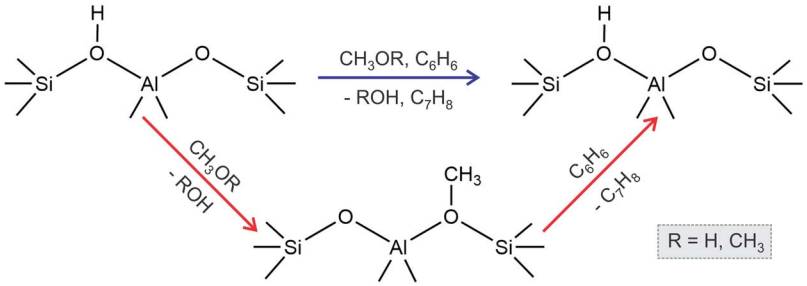

Fig. 1. Schematical representation of the concerted and stepwise methylation mechanisms with MeOH or DME as reactant.

the intermediate release of a water molecule [10,16,17].

Even though most of the methylation kinetic studies are performed under low conversion levels to minimize by-product formation, it remains challenging to limit the occurrence of unwanted secondary reactions. Typical by-products formed during co-feeding of oxygenates with aromatics are polymethyl benzenes (polyMBs), light olefins and the recently reported diphenylmethanes (DPMs) [14]. While polyMBs and olefins are formed by over-methylation and the MTH reaction according to the dual cycle concept [1,2,22], DPM was found to result from Prins-type reactions between benzene and formaldehyde. Formaldehyde is a typical hydrogen-transfer product from methanol–methanol reactions [23–25], or as recently proposed from methanol-alkene reactions at Brønsted or Lewis acid sites [13,26]. While hydrogen transfer between methanol and isobutene and isobutene methylation were found to exhibit similar reaction rates, DME forms a methoxymethyl cation which is higher activated [13]. This results in high DPM selectivities only when using methanol as methylating agent. It should be mentioned that only few studies report on the differences between methanol and DME as methylating agents. Although the chemistry of hydrocarbon methylation with both agents is very similar, there does not seem to be a straightforward trend in reactivity differences between the two. While Maihom et al. report a higher reactivity for methanol [27], other studies conclude that DME is more reactive in H-ZSM-5 [16,28]. Using advanced molecular dynamics simulations, Van der Mynsbrugge et al. concluded that methoxide formation from methanol or dimethyl ether can follow different pathways when assisting molecules are present in the pores of H-ZSM-5. However, methoxide formation from DME was found to exhibit a lower activation energy than from methanol [19].

Recently, systematically higher rates for benzene and isobutene methylation were measured when DME instead of MeOH was used as methylating agent in various zeolites [12,13]. Moreover, also the MTH activity and carbon conversion capacity were found to be higher with a DME feed [15]. While the different deactivation behavior for MTH with a DME and MeOH feed can be explained by different rates of formaldehyde formation and subsequent Prins-type reactions, the higher methylation rates with DME remain an intriguing observation. Therefore, this work focusses on calculating benzene methylation rates at operating conditions from a first principle microkinetic modeling perspective corroborated by detailed kinetic experiments on zeolite nanosheets.

It is striking that many theoretical studies in zeolite catalysis are solely based on (free) energy diagrams, often giving limited insights into the actual performance of the catalyst at operating conditions. In the last years significant progress has been made by introducing the use of advanced molecular dynamics (MD) methods such as metadynamics for zeolite catalysis to study the effect of reaction temperature, pressure, feed composition and zeolite characteristics on elementary reaction steps [10,11,14,19,29,30]. While advanced MD studies led to many unprecedented invaluable insights, they are very time consuming and – especially when using DFT – limited to relatively short time- and length scales. Inspired by the work of Brogaard et al. [16] we instead opt for a microkinetic modeling approach, giving direct access to experimentally measurable rates.

While microkinetic models are nowadays routinely applied in metal (oxide) surface catalysis [31–38], the use of microkinetic models is not widely spread within computational catalysis in nanoporous materials due to often highly complex reaction mechanisms and the high computational expense [39–41]. Moreover, many steady-state microkinetic models make use of a mean-field approximation. By eliminating all possible attractive or repulsive interactions between adsorbates, a uniform coverage of all active sites is assumed, irrespective of their specific location in the catalyst. The only required information is the types of active sites and the elementary processes that can take place at each of them. This simplification is only justified when it can be assumed that there is a perfect mixing of the reaction intermediates over the active sites, e.g. when there is fast diffusion. It is clear that this might be a very limiting approximation in some zeolite materials and if the mean-field assumption breaks down, one has to resort to much more complex kinetic Monte Carlo (kMC) schemes [35,42]. Due to the computational expense and complexity of kMC models, applications have to date been restricted to some seminal works in metal surface catalysis [35,42,43]. In nanoporous materials, kMC applications are currently mostly limited to force-field based diffusion studies [44–48].

In most experimental and theoretical kinetic studies, it is assumed that the oxygenate – either physisorbed on the Brønsted acid site, either converted into a methoxide – completely covers the surface, after which the hydrocarbon weakly co-adsorbs. This, in turn, leads to a representation of the rate law for this elementary reaction step as

$$r = k p_{oxygenate}^{n_{ox}} \; p_{hydrocarbon}^{n_{HC}} \quad (1)$$

in which it is typically assumed that the rate is zeroth order in oxygenate partial pressure ($n_{ox} = 0$), and first order in hydrocarbon partial pressure ($n_{HC} = 1$) [4–7,9,49,50]. Given that the adsorption of the oxygenate, which included the formation of one or more hydrogen bonds, is usually stronger than the co-adsorption of the hydrocarbon, which is mainly driven by long-range dispersion interactions, this is a fair assumption. However, in this work our calculations and kinetic measurements show that this rate expression is only valid in a limited range of temperatures, pressures and feed compositions.

2. Materials and methods

2.1. Computational details

Periodic Density Functional Theory (DFT) calculations were performed using the Vienna Ab Initio Simulation Package (VASP 5.3) with the PBE functional [51–54]. To account for attractive London dispersion interactions, Grimme's D3 corrections were added [55]. During the calculations, the projector augmented wave (PAW) method was used [56,57], a plane-wave cutoff of 600 eV was adopted and the self-consistent field (SCF) convergence criterion was set to 10^{-5} eV. The Brioullin zone sampling was restricted to the Γ-point. Transition states were initially optimized with the improved dimer method and then refined with a quasi-Newton algorithm as implemented in VASP. For the optimization of stable states, a conjugate gradient algorithm was applied.

The H-ZSM-5 catalyst was represented by an orthorhombic unit cell consisting of 96 T atoms containing one substitutional Al defect and charge compensating proton as Brønsted acid site (Fig. S1). The Al substitution is located at the T12 position, similar to earlier work (Fig. S2) [30,58,59], which is at the intersection of the straight and zigzag channel offering maximum available space and creating the most accessible active site. Throughout all simulations, the unit cell parameters are kept fixed at a = 20.02 Å, b = 20.25 Å, c = 13.49 Å, α = 89.87°, β = 89.69°, γ = 90.10°. These values were obtained after a least square fit to the Birch Murnaghan equation of state curve to calculate the optimal unit cell volume as described in earlier work [12]. In all simulations, the location of the BAS was chosen on O20, while methoxides were assumed to form on O24, which is consistent with the work of Van der Mynsbrugge et al. (see Fig. S2) [19]. Note that both oxygens neighbor the aluminum substitution.

To calculate enthalpies and entropies, a partial Hessian vibrational analysis based on the harmonic oscillator (HO) approximation was performed including the guest molecules and proton of the framework (Fig. S3). This subset of atoms was found to be sufficient to study benzene methylation in H-ZSM-5. We repeated the free energy calculations for the concerted reaction while including at 8T cluster of the framework (Fig. S3) and free energies varied less than 5 kJ/mol (see Table S1). As the potential energy surface (PES) is relatively flat, it can be hard to remove all imaginary frequencies as was also pointed out by De Moor et al. [60]. When such superfluous imaginary frequency still appeared after several geometry optimizations with slightly perturbed geometries, this frequency was substituted with an arbitrary value of 50 cm^{-1} as was suggested by De Moor et al. and applied in earlier work [12,13]. The HO approach is known to typically overestimate the entropy losses for adsorbed guest molecules in zeolites and therefore predicts less stable adsorption [61,62]. An important limitation of the HO approximation is that it neglects the often anharmonic character of certain normal modes and nowadays schemes exist to account for this effect. Anharmonic entropies can then be calculated by solving one-dimensional Schrödinger equations for each individual mode as proposed by Piccini et al. [61,63–65] or by calculating a vibrational density of states (VDOS) from molecular dynamics simulations and applying a quasi-harmonic oscillator (QHO) approach.[66] The computational expense of such approaches is much higher than for calculating harmonic vibrational entropies and thorough benchmarking is needed to fully understand the impact of anharmonicity on adsorption, desorption and reactions in zeolites. Therefore, such advanced entropy sampling schemes are not yet widely applied and readily available in popular codes.

The microkinetic model of benzene methylation was evaluated using CatMAP [31] (Version 0.2.270 combines with ASE Version 3.15.0) to obtain a steady-state solution of a set of coupled rate equations corresponding to a series of elementary reaction steps. The model includes adsorption of the oxygenate (MeOH or DME) at the BAS, co-adsorption of benzene, a concerted methyl transfer with water or methanol formation and desorption, methoxide formation with water or methanol formation and desorption followed by benzene co-adsorption, a methyl transfer reaction and finally toluene desorption as listed below.

$$CH_3OR(g) + H^* \leftrightarrow CH_3OR.H^* \quad (2)$$

$$CH_3OR.H^* + C_6H_6(g) \leftrightarrow C_6H_6.CH_3OR.H^* \quad (3)$$

$$C_6H_6.CH_3OR.H^* \leftrightarrow [C_6H_6 - CH_3OR.H^*]^{\ddagger} \leftrightarrow C_7H_8.H^* + ROH(g) \quad (4)$$

$$CH_3OR.H^* \leftrightarrow [CH_3 - OR.H^*]^{\ddagger} \leftrightarrow CH_3^* + ROH(g) \quad (5)$$

$$CH_3^* + C_6H_6(g) \leftrightarrow C_6H_6.CH_3^* \quad (6)$$

$$C_6H_6.CH_3^* \leftrightarrow [C_6H_6 - CH_3^*]^{\ddagger} \leftrightarrow C_7H_8.H^* \quad (7)$$

$$C_7H_8.H^* \leftrightarrow C_7H_8(g) + H^* \quad (8)$$

H* represents the zeolite containing a BAS, X.H* denotes that molecule X is directly interacting with the BAS and R is either H (methanol) or CH_3 (DME). The resulting set of rate equations and differential equations are listed in the Supporting Information. Note that methanol dehydration to DME is not included in the model as experiments to which we compare our model were performed at very low conversions and high space velocities, not allowing the establishment of the MeOH-DME equilibrium. Additionally, adsorption of benzene on the BAS could be included in the model, however, due to the lower adsorption enthalpy of benzene compared to the oxygenates, the coverage of benzene on the BAS is negligible (Fig. S4) and this step is not accounted for in our final results. To avoid the model solution deteriorating to zero proton coverage an arbitrary proton source was added in the model, similarly as done by Brogaard et al. [16] and more details can be found in Section 3 of the Supporting Information.

Based on a list of electronic energies and frequencies, CatMAP computes free energies for all intermediates and transition states, from which rate coefficients and equilibrium constants for reaction steps and adsorption/desorption steps are calculated based on the harmonic transition state theory. Expressions (2–8) result in a set of coupled differential equations (see Supporting Information), from which the coverages of all species at steady-state conditions can be determined. Hereby, conservation of active sites is assumed. Unless stated otherwise, the concentrations of the oxygenate (methanol or DME), benzene, water (or methanol) and toluene were fixed at values of 5.92 10^{-2}, 5.92 10^{-2}, 10^{-5} and 10^{-5} respectively. These values were chosen such that the partial pressures, defined as the concentration times the total pressure, of the oxygenate and benzene at atmospheric pressure (1013.25 mbar) are 60 mbar each. This mimics the experimentally applied feed composition and very low conversion levels of both reactants at experimental conditions (*vide infra*). Experimentally, the feed consists of the reactants and a carrier gas (He) such that the total pressure is around atmospheric pressure. Our model does not account for the presence of the inert carrier gas. The microkinetic model was solved for temperatures in the range of 473.15 − 673.15 K and for pressures ranging from 10^{-1} to 10^{1} bar, forming a bracket around the experimental conditions (*vide infra*).

Eq. (1) represents the general rate law for toluene production. Reaction orders n_{DME} and n_{BZ} for the toluene production rate with respect to the partial pressures of DME and benzene were calculated according to Eqs. (8)–(9).

$$n_{DME} = \frac{d\ \log(r_{toluene})}{d\ \log(p_{DME})} \quad (8)$$

$$n_{BZ} = \frac{d\ \log(r_{toluene})}{d\ \log(p_{BZ})} \quad (9)$$

Degree of rate control as proposed by Campbell and co-workers [67] was applied to identify the reaction step that controls the rate according to Eq. (10).

$$X_{i,j} = \frac{d\ \ln(r_i)}{d\ (-G_j/RT)} \quad (10)$$

With $X_{i,j}$ the rate control matrix, r_i the production rate of product i, G_j the free energy of species j (which is either a stable intermediate or transition state), R the universal gas constant and T the temperature.

2.2. Materials used

A H-ZSM-5 sample with nanosheet morphology has been employed in this work to eliminate diffusion limitations and the occurrence of secondary reactions. The sample was prepared following the protocol described by Ryoo and co-workers [68]. The sample has been characterized and fully described in previous works [12,13]. The experimental Si/Al ratio is 55 corresponding to an average of maximum 2 acid sites per unit cell. The H/Al ratio in the ZSM-5 nanosheets is 0.91

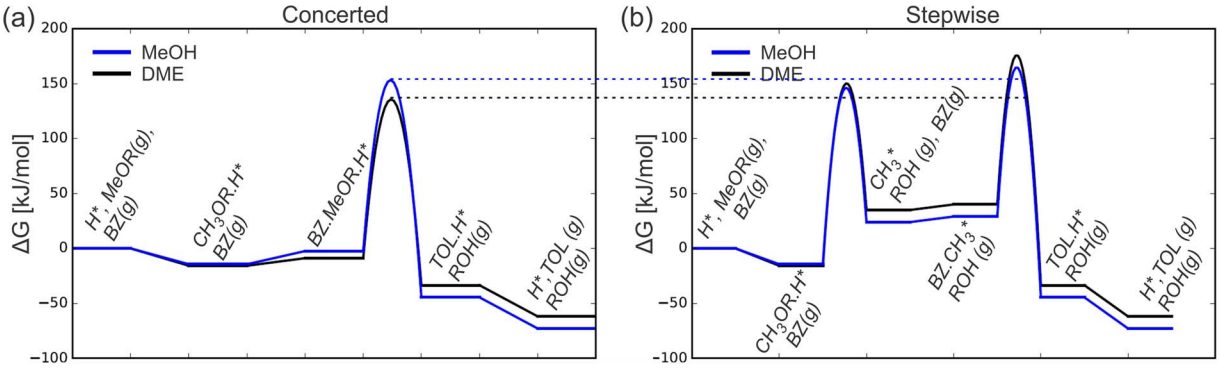

Fig. 2. Free energy diagrams (kJ/mol) at 350 °C for the concerted (a) and stepwise (b) methylation of benzene my methanol (blue) and dimethyl ether (black). H* stands for the zeolite surface containing a Brønsted acid site, MeOR stands for methanol (R=H) or dimethyl ether (R=CH_3), BZ stand for benzene and TOL for toluene. (For interpretation of the references to colour in this figure legend, the reader is referred to the web version of this article.)

indicating that most of the Al is incorporated in the framework with the creation of bridging OH groups as Brønsted acid sites. The theoretical zeolite unit cell has 1 Al and 95 Si atoms and thus 1 BAS (*vide supra*). Given that the MFI unit cell of ZSM-5 is relatively large, it is a fair assumption that a ratio of 55 corresponds to isolated Brønsted acid site, suggesting that theory and experiment describe similar materials. Further acidic and textural properties are presented in Table S2.

2.3. Catalytic testing

MeOH (VWR, 99.8%), DME (AGA, 25 mol% DME/argon 6.0) and benzene (Sigma-Aldrich Chroma Solv, 99.9%) were used as reactants. Liquid reactants were fed by flowing a He stream through a flask of boiling reactant. The saturated helium stream was then passed upwards through a water-cooled Vigreux condenser kept at constant temperature (30 °C for MeOH and 35 °C for benzene). The desired reactant partial pressure was obtained by adjusting the total flow of the reactants and a third gas line with pure He.

All catalytic tests were carried out in a fixed bed quartz reactor (inner diameter 8 mm) at atmospheric pressure. Catalyst powder and inert quartz were pressed and sieved to 250–420 μm. Temperatures were monitored using a thermocouple covered by a 3 mm wide quartz sleeve placed above the catalyst bed. The samples were activated by heating in 20% O_2/He to 550 °C with a 5 °C/min ramp, and temperature was kept at 550 °C in 100% O_2 for 1 h. Then, the reactor was cooled to reaction temperature at 5 °C/min in He flow. Catalytic tests used 5 mg of H-ZSM-5 catalyst diluted with 40 mg quartz. Benzene was co-reacted with either MeOH or DME with partial pressures ranging from 10 mbar to 80 mbar at 250–350 °C and a total flow equal to 100 mL/min. Benzene conversion was below 14% in all cases. We systematically checked that benzene conversion fits with the methanol fraction in the effluent after every methylation event by DME. Therefore, we are assured that DME acts as a single methylating agent under the experimental conditions tested.

The reaction effluent was analyzed after 10 min of reaction by online GC/MS instrument (Agilent 7890 with flame ionization detector and 5975C MS detector) using two Restek Rtx-DHA-150 columns.

3. Results and discussion

The aim of our microkinetic model is to calculate toluene production rates from benzene methylation by MeOH or DME over H-ZSM-5 at operating conditions. To calculate the rate and equilibrium constants of all elementary steps listed in the computational section, a set of raw DFT data consisting of electronic energies and frequencies is converted into relevant thermodynamic quantities. Free energies are the backbone of the microkinetic model and free energy diagrams at 350 °C for concerted and stepwise benzene methylation by MeOH or DME over H-ZSM-5 are presented in Fig. 2. The reference state is chosen as the zeolite surface containing Brønsted acid sites (H*) and the oxygenate and benzene in gas phase.

For the concerted methylation, a difference in the overall free energy barrier at 350 °C between methanol and DME as methylating agent of ca. 18 kJ/mol is found, with DME exhibiting the lowest barrier. This suggests that methylation rates with DME are significantly faster than with MeOH due to a different co-adsorption strength of benzene with the oxygenates at the BAS and differences in the intrinsic barriers. Brogaard et al. made similar observations for alkene methylations in H-ZSM-22, attributing the higher reactivity of DME to a better stabilization of the concerted methylation transition states due to additional electrostatic stabilization by the additional methyl group [16]. It can be expected that similar effects are at play here. Note that our static calculations start from favorable pre-reactive complexes in which the methyl group of methanol or DME points towards benzene. Hence, we do not account for the different probabilities for methanol and DME for adopting such favorable orientations as observed with ab initio molecular dynamics simulations [12].

While methoxide formation from both oxygenates exhibits similar free energy barriers as the concerted reaction, the overall free energy barrier for stepwise methylation is slightly higher than for the concerted reaction. At 350 °C the difference in overall free energy barrier between both mechanisms is lower for methanol than for DME, suggesting that at 350 °C stepwise methylation is more important with a methanol feed than with a DME feed. Methoxide formation at 350 °C from both oxygenates exhibits nearly equal barriers, which is in line with earlier reported static DFT calculations [19,20]. A full list of free energies is included in the Supporting Information (Table S3 and Table S4).

Solving the mean-field microkinetic model results in toluene production rates as displayed in Fig. 3. For low temperatures, the toluene production rate is significantly higher for DME than for MeOH, however the difference becomes smaller with increasing temperature and decreasing total pressure.

By co-feeding the oxygenates with benzene (60:60 mbar) over H-ZSM-5 nanosheets, the net product formation rates could be measured at various temperatures as shown in Fig. 4. The primary and most abundant product is toluene; however, also side-products are formed including polymethylated benzenes (PMBs) due to over-methylation, diphenyl methane (DPM) due to hydrogen transfer reactions and Prins-type reactions between formaldehyde and benzene as discussed elsewhere [12], and aliphatics due to initiation of the hydrocarbon pool for MTH chemistry. As discussed in earlier work, DME is much more selective towards methylation than MeOH due to less competition with hydrogen transfer reactions [12,13].

Toluene formation rates with DME are significantly higher than with MeOH and the difference becomes smaller with increasing

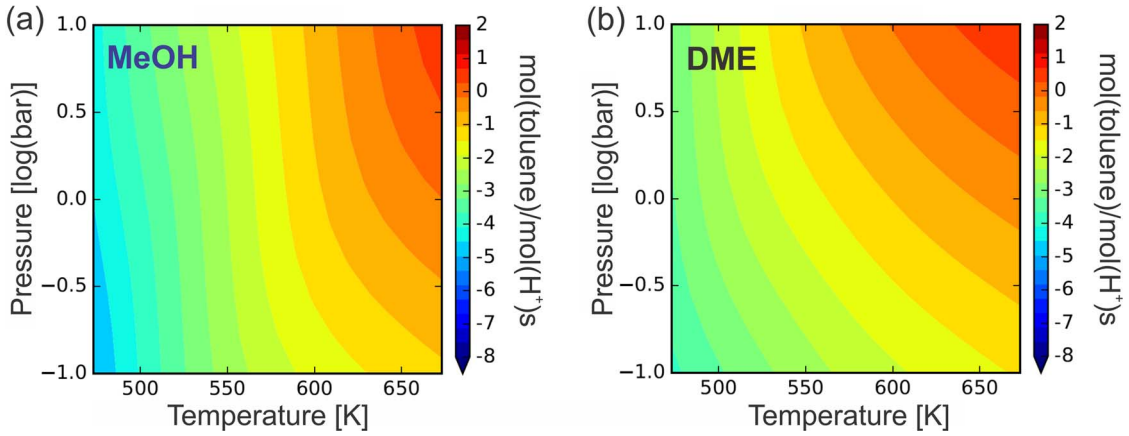

Fig. 3. Toluene production rates expressed in mol(toluene)/mol(H*)s (log scale) as a function of temperature (K) and pressure (log scale, in bar) for benzene methylation by MeOH (a) and DME (b).

temperature. This is in good agreement with the calculated toluene production rates shown in Fig. 3.

Table 1 summarizes the calculated and measured toluene production rates at 250, 300 and 350 °C. The model is also able to reproduce the relative rates for DME versus MeOH fairly well. Especially for low temperatures (250 and 300 °C), the agreement between the theoretical and experimental DME/MeOH ratio in terms of toluene production rate is very good. At 350 °C, the DFT based microkinetic model predicts a slightly higher rate for methylation by MeOH than by DME, which is not observed in the experiments. As the stepwise mechanism significantly contributes to the rate at high temperature (vide infra), this might indicate that the DFT data of methoxide formation from MeOH and DME are slightly less accurate than for the other reactions. It should be noted that Van der Mynsbrugge et al. reported based on ab initio metadynamics that the free energy barrier at 350 °C for methoxide formation from DME is 17 kJ/mol lower than for MeOH when no assisting molecules are at play [19]. In the same work, static calculations on finite cluster models resulted in similar barriers for the reaction with DME or MeOH. Our current periodic DFT results are in agreement with those static results from Van der Mynsbrugge et al.

For a DME feed, accurate activation energies and apparent enthalpy barriers could be calculated from experimental Arrhenius plots. These values are in very good agreement with the calculated values (Fig. S5 and Table S5). Given that our model does not include any secondary reaction steps, relies on DFT calculations at a relatively inexpensive PBE-D3 level of theory and makes use of the harmonic transition state theory, the relatively good agreement between theory and experiment suggests that our methodology is capable of capturing the most important trends observed during the experimental measurements. DFT data based on more advanced functionals or including anharmonic partition functions (cfr. Computational details), would increase the accuracy of the model but this is beyond the scope of the current study.

To determine the operating conditions for which the concerted or stepwise mechanism is dominating in our microkinetic model, we apply the concept of degree of rate control. This concept provides a rigorous way to identify the rate determining transition states and intermediates.

Table 1
Calculated (DFT) and measured (Exp.) toluene production rates for benzene methylation with MeOH or DME over H-ZSM-5 at 250, 300 and 350 °C with a 60:60 mbar oxygenate:benzene feed composition.

Production rate [mol TOL/molH*h]	MeOH		DME		DME/MeOH	
	DFT	Exp.	DFT	Exp.	DFT	Exp.
250 °C	3	10	31	69	10.3	6.9
300 °C	66	77	167	268	2.5	3.5
350 °C	653	315	565	714	0.9	2.3

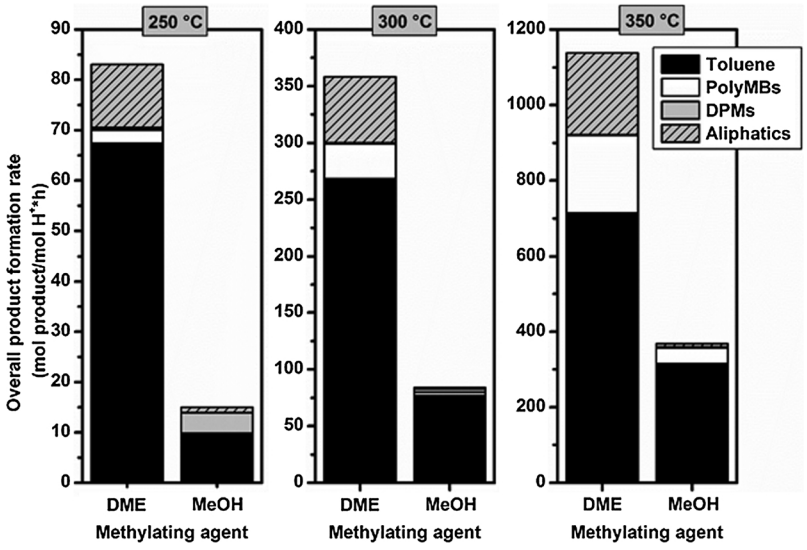

Fig. 4. Net product formation rate during benzene co-reaction with methanol or DME (60:60 mbar) over H-ZSM-5 at 250, 300 and 350 °C. Total flow = 100 mL/min. Benzene conversion < 9%.

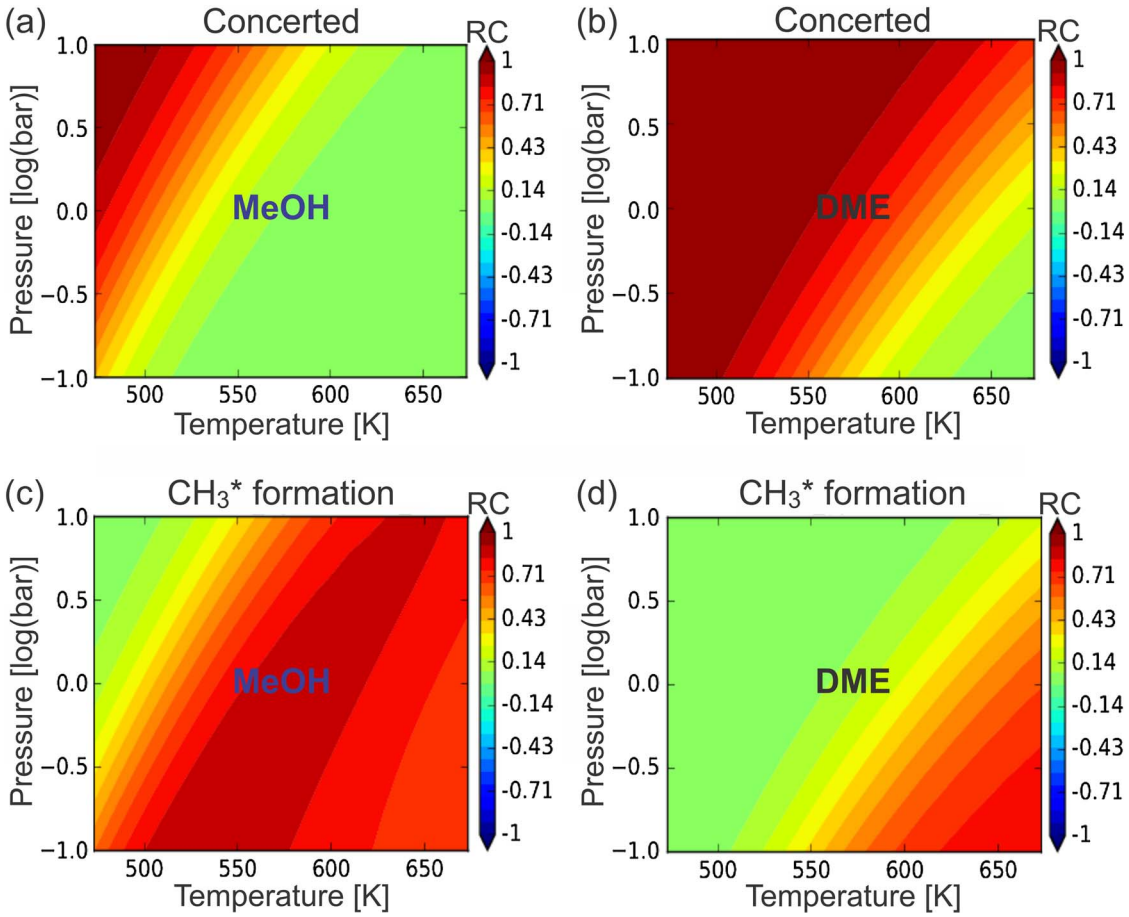

Fig. 5. Degree of rate control (RC) for toluene formation by the transition state of the concerted (a,b) and first step of the stepwise (c,d) mechanism for benzene methylation with MeOH (a,c) and DME (b,d) over H-ZSM-5.

While the adsorption of the oxygenates and benzene definitely impact the methylation rate, we focus on the degree of rate control with respect to the free energies of the transition state of the concerted methylation and the transition state for methoxide formation (Fig. 5). All other transition states or stable states were found to have less impact on the rate. From Fig. 5 it can be concluded that an expected shift from the concerted to the stepwise mechanism takes place with increasing temperature and decreasing pressure due to the entropic gain related to the intermediate release of a water or methanol molecule upon methoxide formation. The transition occurs at higher pressures and lower temperatures for methanol than for DME. This transition of methylation mechanism has been reported before based on DFT microkinetic models, advanced molecular dynamics and experiments for alkene methylation and methanol dehydration reactions [16,17]. Note that this analysis also shows that methoxide formation is the rate determining step for the stepwise mechanism as the degree of rate control of the transition state of the second step was close to zero. Our experiments were performed at temperatures ranging from 250 °C to 350 °C and at ambient pressure, hence the measured product formation rates from DME mostly correspond to the concerted reaction, while the stepwise mechanism already has a significant contribution with a MeOH feed at these conditions.

Next to the intrinsically lower free energy barrier for the concerted reaction with DME (see Fig. 2), the slightly different transition point for the methylation mechanism explains why the differences in reactivity of MeOH and DME become smaller with increasing temperature as the stepwise mechanism provides an acceleration of the methylation rates. Our findings thus suggest that methylation rates at higher temperatures become less dependent of the substrate. It should also be noted that typical MTH temperatures are 350 °C or higher, meaning that under MTH conditions stepwise methylations might be important.

As we observe a shift in the dominant methylation mechanism with varying operating conditions, it is highly questionable whether the traditionally assumed rate law with zeroth order in the oxygenate partial pressure and first order in the hydrocarbon partial pressure is always valid. Therefore, we calculated reaction orders for DME and benzene from our microkinetic model. The results shown in Fig. 6(a,b) suggest that at ambient pressure and when using a 60:60 mbar DME:-benzene feed, zeroth order in DME and (nearly) first order in benzene is only achieved for a narrow temperature range (roughly between 525 and 575 K). At higher temperatures, the coverage of DME decreases and due to the contribution of the competing stepwise mechanism, partial reaction orders are expected. This effect is even more pronounced for a MeOH feed resulting in low benzene reaction orders as shown in Fig. S6.

The occurrence of partial reaction orders was confirmed by DME-benzene co-feeding experiments in which either the DME or benzene partial pressure was varied (Fig. 7). According to equation (1), when plotting the logarithm of the rate of benzene conversion versus the logarithm of the partial pressure of each reactant, the respective reaction orders can be determined. It is noted that secondary reactions are difficult to be avoided under experimental conditions despite of the differential conditions achieved (benzene conversion < 14%). The use of rate of benzene conversion instead of net toluene production aims to account for the most abundant by-products, xylenes, which have been formed via sequential benzene methylation. From the slopes in Fig. 7 it can be concluded that there is no zeroth order in DME and no first order in benzene. For DME, the slope decreases with increasing DME partial

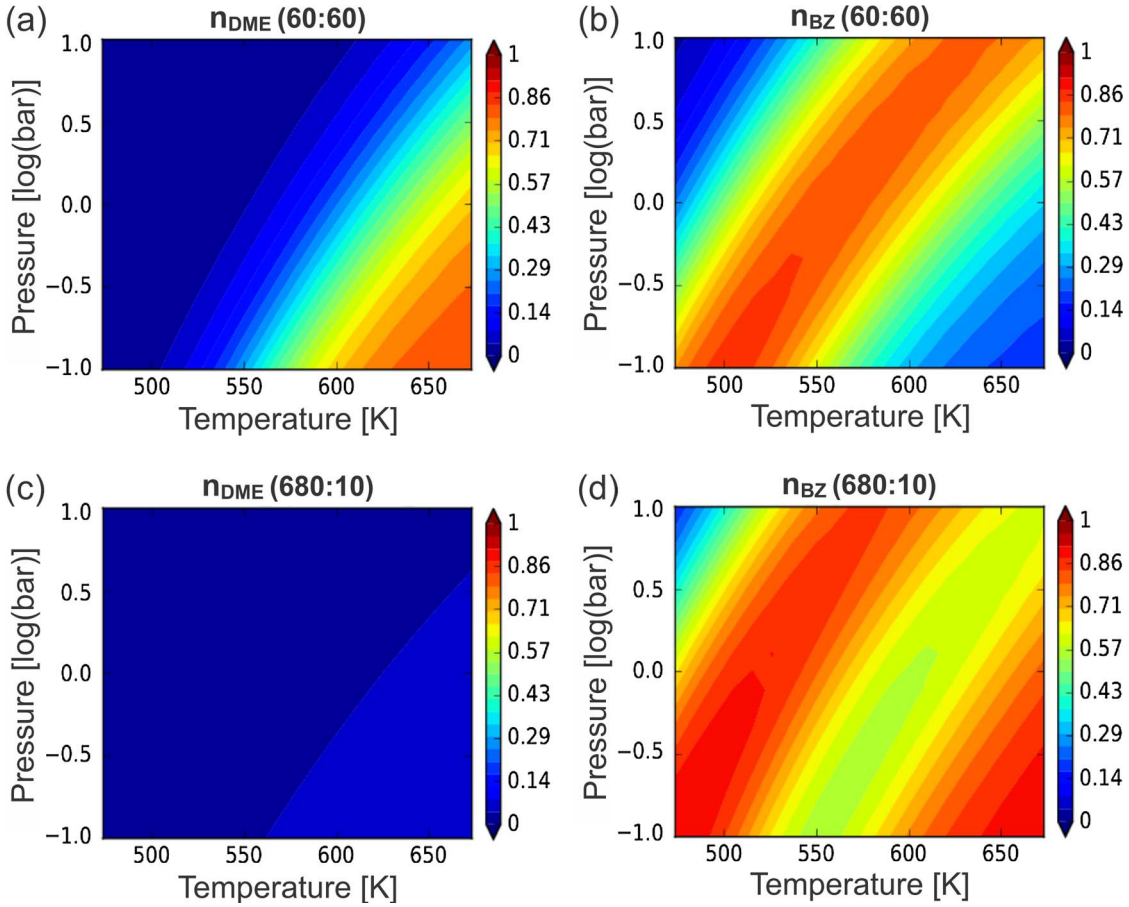

Fig. 6. Reaction order with respect to DME partial pressure (a) and benzene partial pressure (b) for benzene methylation with DME over H-ZSM-5 as a function of operating conditions.

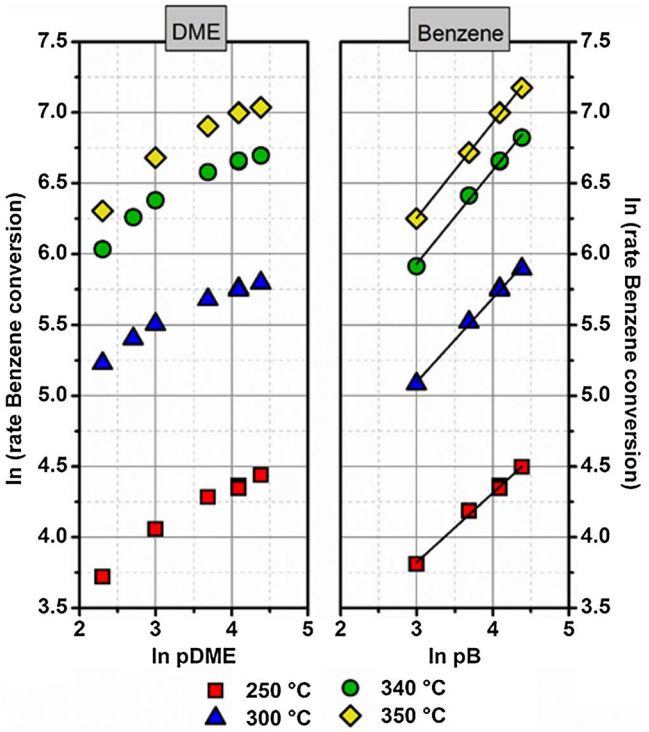

Fig. 7. Correlation of partial pressure of DME and benzene with benzene conversion rate during co-feeding benzene:DME over H-ZSM-5 at 250–350 °C. Left: co-reaction benzene:DME (60:10–80 mbar). Right: benzene:DME (20–80:60 mbar). Total flow = 100 mL/min. Benzene conversion < 14%.

pressure, suggesting that for a feed with higher DME than benzene partial pressures, the reaction order of DME is closer to the traditional zeroth order.

The reaction orders calculated from the microkinetic model and obtained from the experiments are summarized in Table 2. The DFT and experimental data both show partial reaction orders for DME and benzene, but no full quantitative agreement is obtained. It should be noted that there are significant error bars on both theoretical and experimental values. While reaction orders calculated according to equations (8) and (9) only account for infinitesimal variations of the 60:60 mbar DME:benzene feed composition, the experimental values are derived from co-feeding experiments with feed compositions varying between 10-80:60 mbar DME:benzene for n_{DME} and 60:20–80 mbar DME:benzene for n_{BZ}. Next to deviations due to inherent errors on DFT based results, the theoretical reaction orders are also highly sensitive to the exact feed composition as shown in Table S6.

Table 2
Calculated (DFT) and measured (Exp.) reaction orders for DME (n_{DME}) and benzene (n_{BZ}) partial pressure for benzene methylation with DME over H-ZSM-5 at 250 °C and 350 °C. In the microkinetic model a 60:60 mbar DME:benzene or a 680:10 mbar DME:benzene feed was used. Experimentally the feed composition was varied between 10-80:60 mbar DME:benzene for n_{DME} and 60:20–80 mbar DME:benzene for n_{BZ}.

Reaction order	DFT (60:60)		Exp.		DFT (680:10)	
	n_{DME}	n_{BZ}	n_{DME}	n_{BZ}	n_{DME}	n_{BZ}
250 °C	0.01	0.71	0.34	0.5	0.00	0.88
300 °C	0.10	0.81	0.27	0.59	0.01	0.67
350 °C	0.42	0.58	0.35	0.67	0.04	0.61

The results in Figs. 6 and 7 and Table 2 clearly suggest that caution is warranted when assuming the traditional rate law for methylation reactions as its validity depends on the applied operating conditions. Previous studies on kinetics of methylation reactions in H-ZSM-5 often report a very clear zeroth order for the oxygenate and first order for the hydrocarbon [3,4,9,16,69,70]. In all these studies, the oxygenate partial pressure was always significantly higher than the hydrocarbon partial pressure. Inspired by these observations, we solved the microkinetic model with concentrations of 0.6711 and 0.00987 for DME and benzene respectively, corresponding to a 680:10 mbar feed at ambient pressure as applied in the work of Bhan and co-workers [4]. The reaction orders for DME and benzene are shown in Fig. 6(c,d) and clearly show a different behavior compared to a 60:60 mbar DME:benzene feed composition. Especially at low temperature, we observe a zeroth order for DME and a benzene reaction order that is closer to 1 compared to the 60:60 mbar DME:benzene feed. For methanol, a similar effect is observed when using a 680:10 mbar methanol-benzene feed (Fig. S6). These results demonstrate that next to temperature and pressure also feed composition is a crucial parameter for kinetic studies that needs to be carefully incorporated in microkinetic models by properly choosing the relative pressures of all gas phase molecules.

4. Conclusions

Herein we show that a DFT based microkinetic model of benzene methylation by methanol and dimethyl ether in H-ZSM-5 is capable of predicting trends in toluene formation rates in relatively good agreement with experimental data. We find that toluene production rates from DME are approximately an order of magnitude higher than from MeOH due to subtle differences in coverage of reactants and a better stabilization of the cationic transition state for the concerted reaction step with DME. The differences in reactivity between DME and MeOH decrease with increasing temperature due to contributions of the stepwise mechanism at higher temperatures. With increasing temperature and decreasing pressure a shift from the concerted to stepwise methylation mechanism is observed and this transition occurs at lower temperatures for MeOH.

Our microkinetic model shows that the traditional rate law for zeolite-catalyzed methylation reactions assuming a zeroth order in the oxygenate partial pressure and first order in the hydrocarbon partial pressure is not universally valid. We find that the applied temperature and pressure have a major influence as the dominant methylation mechanism depends on the operating conditions. Consequently, partial reaction orders are observed for both reactants for a broad range of operating conditions. Only when using a feed with high oxygenate partial pressure compared to benzene partial pressure we find the traditional rate law in a broader range of temperatures and pressures.

While it is common practice in zeolite catalysis to limit kinetic studies to a detailed analysis of free energy diagrams, this study – in line with earlier literature reports in this field – underlines the importance of accounting for operating conditions in DFT based microkinetic models. Due to the good agreement with experimental data, this work paves the way to more complex microkinetic studies of mechanisms that are representative for MTH chemistry based on a similar methodology.

Conflicts of interest

None.

Acknowledgements

KDW acknowledges the Belgian American Educational Foundation (BAEF) and the Research Foundation Flanders (FWO). KDW, MJH, TB are grateful for support from the DOE Office of Basic Energy Science to the SUNCAT Center for Interface Science and Catalysis. Part of the computational resources and services used were provided by Ghent University (Stevin Supercomputer Infra-structure) and the VSC (Flemish Supercomputer Center), funded by the Research Foundation – Flanders (FWO). JSME, SS, UO acknowledge the financial support received via the European Industrial Doctorates project “ZeoMorph” (FP7 ITN-EID), part of the Marie Curie actions (grant agreement no-606965).

Appendix A. Supplementary data

Supplementary data associated with this article can be found, in the online version, at https://doi.org/10.1016/j.cattod.2018.02.042.

References

[1] U. Olsbye, S. Svelle, M. Bjørgen, P. Beato, T.V.W. Janssens, F. Joensen, S. Bordiga, K.P. Lillerud, Conversion of methanol to hydrocarbons: how zeolite cavity and pore size controls product selectivity, Angew. Chem. Int. Edit. 51 (2012) 5810–5831.
[2] K. Hemelsoet, J. Van der Mynsbrugge, K. De Wispelaere, M. Waroquier, V. Van Speybroeck, Unraveling reaction mechanisms governing methanol-to-olefins catalysis combining theory with experiment, ChemPhysChem 14 (2013) 1526–1545.
[3] S. Svelle, M. Visur, U. Olsbye, M. Bjørgen, Saepurahman, Mechanistic aspects of the zeolite catalyzed methylation of alkenes and aromatics with methanol: a review, Top. Catal. 54 (2011) 897–906.
[4] I.M. Hill, A. Malek, A. Bhan, Kinetics and mechanism of benzene, toluene, and xylene methylation over H-MFI, ACS Catal. 3 (2013) 1992–2001.
[5] I.M. Hill, S. Al Hashimi, A. Bhan, Kinetics and mechanism of olefin methylation reactions on zeolites, J. Catal. 285 (2012) 115–123.
[6] I.M. Hill, Y.S. Ng, A. Bhan, Kinetics of butene isomer methylation with dimethyl ether over zeolite catalysts, ACS Catal. 2 (2012) 1742–1748.
[7] V. Van Speybroeck, J. Van der Mynsbrugge, M. Vandichel, K. Hemelsoet, D. Lesthaeghe, A. Ghysels, G.B. Marin, M. Waroquier, First principle kinetic studies of zeolite-catalyzed methylation reactions, J. Am. Chem. Soc. 133 (2011) 888–899.
[8] S. Svelle, C. Tuma, X. Rozanska, T. Kerber, J. Sauer, Quantum chemical modeling of zeolite-catalyzed methylation reactions: toward chemical accuracy for barriers, J. Am. Chem. Soc. 131 (2009) 816–825.
[9] J. Van der Mynsbrugge, M. Visur, U. Olsbye, P. Beato, M. Bjørgen, V. Van Speybroeck, S. Svelle, Methylation of benzene by methanol: single-site kinetics over H-ZSM-5 and H-beta zeolite catalysts, J. Catal. 292 (2012) 201–212.
[10] K. De Wispelaere, S. Bailleul, V. Van Speybroeck, Towards molecular control of elementary reactions in zeolite catalysis by advanced molecular simulations mimicking operating conditions, Catal. Sci. Technol. 6 (2016) 2686–2705.
[11] K. De Wispelaere, B. Ensing, A. Ghysels, E.J. Meijer, V. Van Speybroeck, Complex reaction environments and competing reaction mechanisms in zeolite catalysis: insights from advanced molecular dynamics, Chem. −Eur. J. 21 (2015) 9385–9396.
[12] J.S. Martínez-Espín, K. De Wispelaere, M. Westgård Erichsen, S. Svelle, T.V.W. Janssens, V. Van Speybroeck, P. Beato, U. Olsbye, Benzene co-reaction with methanol and dimethyl ether over zeolite and zeotype catalysts: evidence of parallel reaction paths to toluene and diphenylmethane, J. Catal. 349 (2017) 136–148.
[13] J.S. Martínez-Espín, K. De Wispelaere, T.V.W. Janssens, S. Svelle, K.P. Lillerud, P. Beato, V. Van Speybroeck, U. Olsbye, Hydrogen transfer versus methylation: on the genesis of aromatics formation in the Methanol-To-Hydrocarbons over H-ZSM-5, ACS Catal. 7 (2017) 5773–5780.
[14] M. Westgård Erichsen, K. De Wispelaere, K. Hemelsoet, S.L.C. Moors, T. Deconinck, M. Waroquier, S. Svelle, V. Van Speybroeck, U. Olsbye, How zeolitic acid strength and composition alter the reactivity of alkenes and aromatics towards methanol, J. Catal. 328 (2015) 186–196.
[15] J.S. Martínez-Espín, M. Morten, T.V.W. Janssens, S. Svelle, P. Beato, U. Olsbye, New insights into catalyst deactivation and product distribution of zeolites in the methanol-to-hydrocarbons (MTH) reaction with methanol and dimethyl ether feeds, Catal. Sci. Technol. 7 (2017) 2700–2716.
[16] R.Y. Brogaard, R. Henry, Y. Schuurman, A.J. Medford, P.G. Moses, P. Beato, S. Svelle, J.K. Nørskov, U. Olsbye, Methanol-to-hydrocarbons conversion: the alkene methylation pathway, J. Catal. 314 (2014) 159–169.
[17] A.J. Jones, E. Iglesia, Kinetic, spectroscopic, and theoretical assessment of associative and dissociative methanol dehydration routes in zeolites, Angew. Chem. Int. Ed. 53 (2014) 12177–12181.
[18] A.M. Vos, K.H.L. Nulens, F. De Proft, R.A. Schoonheydt, P. Geerlings, Reactivity descriptors and rate constants for electrophilic aromatic substitution: acid zeolite catalyzed methylation of benzene and toluene, J. Phys. Chem. B 106 (2002) 2026–2034.
[19] J. Van der Mynsbrugge, S.L.C. Moors, K. De Wispelaere, V. Van Speybroeck, Insight into the formation and reactivity of framework-bound methoxide species in H-ZSM-5 from static and dynamic molecular simulations, ChemCatChem 6 (2014) 1906–1918.
[20] A. Ghorbanpour, J.D. Rimer, L.C. Grabow, Computational assessment of the dominant factors governing the mechanism of methanol dehydration over H-ZSM-5 with heterogeneous aluminum distribution, ACS Catal. 6 (2016) 2287–2298.
[21] P.G. Moses, J.K. Nørskov, Methanol to dimethyl ether over ZSM-22: a periodic density functional theory study, ACS Catal. 3 (2013) 735–745.
[22] S. Svelle, F. Joensen, J. Nerlov, U. Olsbye, K.P. Lillerud, S. Kolboe, M. Bjørgen, Conversion of methanol into hydrocarbons over zeolite H-ZSM-5: Ethene formation

is mechanistically separated from the formation of higher alkenes, J. Am. Chem. Soc. 128 (2006) 14770–14771.
[23] Z.H. Wei, Y.Y. Chen, J.F. Li, W.P. Guo, S. Wang, M. Dong, Z.F. Qin, J.G. Wang, H.J. Jiao, W.B. Fan, Stability and reactivity of intermediates of methanol related reactions and CC bond formation over H-ZSM-5 acidic catalyst: a computational analysis, J. Phys. Chem. C 120 (2016) 6075–6087.
[24] Z.H. Wei, Y.Y. Chen, J.F. Li, P.F. Wang, B.Q. Jing, Y. He, M. Dong, H.J. Jiao, Z.F. Qin, J.G. Wang, W.B. Fan, Methane formation mechanism in the initial methanol-to-olefins process catalyzed by SAPO-34, Catal. Sci. Technol. 6 (2016) 5526–5533.
[25] D. Lesthaeghe, V. Van Speybroeck, G.B. Marin, M. Waroquier, Understanding the failure of direct C-C coupling in the zeolite-catalyzed methanol-to-olefin process, Angew. Chem. Int. Ed. 45 (2006) 1714–1719.
[26] S. Müller, Y. Liu, F.M. Kirchberger, M. Tonigold, M. Sanchez-Sanchez, J.A. Lercher, Hydrogen transfer pathways during zeolite catalyzed methanol conversion to hydrocarbons, J. Am. Chem. Soc. 138 (2016) 15994–16003.
[27] T. Maihom, B. Boekfa, J. Sirijaraensre, T. Nanok, M. Probst, J. Limtrakul, Reaction mechanisms of the methylation of ethene with methanol and dimethyl ether over H-ZSM-5: an ONIOM study, J. Phys. Chem. C 113 (2009) 6654–6662.
[28] S. Svelle, S. Kolboe, O. Swang, U. Olsbye, Methylation of alkenes and methylbenzenes by dimethyl ether or methanol on acidic zeolites, J. Phys. Chem. B 109 (2005) 12874–12878.
[29] K. De Wispelaere, C.S. Wondergem, B. Ensing, K. Hemelsoet, E.J. Meijer, B.M. Weckhuysen, V. Van Speybroeck, J. Ruiz-Martínez, Insight into the effect of water on the methanol-to-olefins conversion in H-SAPO-34 from molecular simulations and in situ microspectroscopy, ACS Catal. 6 (2016) 1991–2002.
[30] S.L.C. Moors, K. De Wispelaere, J. Van der Mynsbrugge, M. Waroquier, V. Van Speybroeck, Molecular dynamics kinetic study on the zeolite-catalyzed benzene methylation in ZSM-5, ACS Catal. 3 (2013) 2556–2567.
[31] A.J. Medford, C. Shi, M.J. Hoffmann, A.C. Lausche, S.R. Fitzgibbon, T. Bligaard, J.K. Nørskov, CatMAP. a software package for descriptor-based microkinetic mapping of catalytic trends, Catal. Lett. 145 (2015) 794–807.
[32] A.J. Medford, A. Vojvodic, J.S. Hummelshøj, J. Voss, F. Abild-Pedersen, F. Studt, T. Bligaard, A. Nilsson, J.K. Nørskov, From the Sabatier principle to a predictive theory of transition-metal heterogeneous catalysis, J. Catal. 328 (2015) 36–42.
[33] L.C. Grabow, F. Studt, F. Abild-Pedersen, V. Petzold, J. Kleis, T. Bligaard, J.K. Nørskov, Descriptor-based analysis applied to HCN synthesis from NH3 and CH4, Angew. Chem. Int. Ed. 50 (2011) 4601–4605.
[34] A.A. Latimer, A.R. Kulkarni, H. Aljama, J.H. Montoya, J.S. Yoo, C. Tsai, F. Abild-Pedersen, F. Studt, J.K. Nørskov, Understanding trends in CH bond activation in heterogeneous catalysis, Nat. Mater. 16 (2017) 225–229.
[35] M.K. Sabbe, M.F. Reyniers, K. Reuter, First-principles kinetic modeling in heterogeneous catalysis: an industrial perspective on best-practice, gaps and needs, Catal. Sci. Technol. 2 (2012) 2010–2024.
[36] A. Banerjee, A.P. van Bavel, H. Kuipers, M. Saeys, CO activation on realistic cobalt surfaces: kinetic role of hydrogen, ACS Catal. 7 (2017) 5289–5293.
[37] I.A.W. Filot, R.J.P. Broos, J.P.M. van Rijn, G. van Heugten, R.A. van Santen, E.J.M. Hensen, First-principles-based microkinetics simulations of synthesis gas conversion on a stepped rhodium surface, ACS Catal. 5 (2015) 5453–5467.
[38] N. López, N. Almora-Barrios, G. Carchini, P. Blonski, L. Bellarosa, R. Garcia-Muelas, G. Novell-Leruth, M. Garcia-Mota, State-of-the-art and challenges in theoretical simulations of heterogeneous catalysis at the microscopic level, Catal. Sci. Technol. 2 (2012) 2405–2417.
[39] C.M. Wang, R.Y. Brogaard, B.M. Weckhuysen, J.K. Nørskov, F. Studt, Reactivity descriptor in solid acid catalysis: predicting turnover frequencies for propene methylation in zeotypes, J. Phys. Chem. Lett. 5 (2014) 1516–1521.
[40] C. Wang, R.Y. Brogaard, Z. Xie, F. Studt, Transition-state scaling relations in zeolite catalysis: influence of framework topology and acid-site reactivity, Catal. Sci. Technol. 5 (2015) 2814–2820.
[41] R.Y. Brogaard, C.-M. Wang, F. Studt, Methanol–alkene reactions in zeotype acid catalysts: insights from a descriptor-based approach and microkinetic modeling, ACS Catal. (2014) 4504–4509.
[42] K. Reuter, M. Scheffler, First-principles kinetic Monte Carlo simulations for heterogeneous catalysis: application to the CO oxidation at RuO2(110), Phys. Rev. B 73 (2006) 17.
[43] K. Reuter, Ab initio thermodynamics and first-principles microkinetics for surface catalysis, Catal. Lett. 146 (2016) 541–563.
[44] A.R. Teixeira, X.D. Qi, W.C. Conner, T.J. Mountziaris, W. Fan, P.J. Dauenhauer, 2D surface structures in small zeolite MFI crystals, Chem. Mat. 27 (2015) 4650–4660.
[45] S.E. Jee, D.S. Sholl, Carbon dioxide and methane transport in DDR zeolite: insights from molecular simulations into carbon dioxide separations in small pore zeolites, J. Am. Chem. Soc. 131 (2009) 7896–7904.
[46] A. Gupta, R.Q. Snurr, A study of pore blockage in silicalite zeolite using free energy perturbation calculations, J. Phys. Chem. B 109 (2005) 1822–1833.
[47] R. Krishna, D. Paschek, R. Baur, Modeling the occupancy dependence of diffusivities in zeolites, Microporous Mesoporous Mat. 76 (2004) 233–246.
[48] B. Smit, R. Krishna, Monte Carlo simulations in zeolites, Curr. Opin. Solid State Mater. Sci. 5 (2001) 455–461.
[49] M. Piccini, Ab initio calculation of rate constants for molecule–surface reactions with chemical accuracy, Angew. Chem. Int. Ed. 55 (2016) 5235–5237.
[50] J. Van der Mynsbrugge, J. De Ridder, K. Hemelsoet, M. Waroquier, V. Van Speybroeck, Enthalpy and entropy barriers explain the effects of topology on the kinetics of zeolite-catalyzed reactions, Chem. −Eur. J. 19 (2013) 11568–11576.
[51] G. Kresse, J. Furthmuller, Efficient iterative schemes for ab initio total-energy calculations using a plane-wave basis set, Phys. Rev. B 54 (1996) 11169–11186.
[52] G. Kresse, J. Furthmuller, Efficiency of ab-initio total energy calculations for metals and semiconductors using a plane-wave basis set, Comput. Mater. Sci. 6 (1996) 15–50.
[53] G. Kresse, J. Hafner, Ab initio molecular-dynamics simulation of the liquid-metal amorphous-semiconductor transition in germanium, Phys. Rev. B 49 (1994) 14251–14269.
[54] G. Kresse, J. Hafner, Ab initio molecular dynamics for liquid metals, Phys. Rev. B 47 (1993) 558–561.
[55] S. Grimme, J. Antony, S. Ehrlich, H. Krieg, A consistent and accurate ab initio parametrization of density functional dispersion correction (DFT-D) for the 94 elements H-Pu, J. Chem. Phys. 132 (2010) 19.
[56] G. Kresse, D. Joubert, From ultrasoft pseudopotentials to the projector augmented-wave method, Phys. Rev. B 59 (1999) 1758–1775.
[57] P.E. Blochl, Projector augmented-wave method, Phys. Rev. B 50 (1994) 17953–17979.
[58] J. Hajek, J. Van der Mynsbrugge, K. De Wispelaere, P. Cnudde, L. Vanduyfhuys, M. Waroquier, V. Van Speybroeck, On the stability and nature of adsorbed pentene in Brønsted acid zeolite H-ZSM-5 at 323 K, J. Catal. 340 (2016) 227–235.
[59] J. Van der Mynsbrugge, S.L.C. Moors, K. De Wispelaere, V. Van Speybroeck, Insight into the formation and reactivity of framework-bound methoxide species in H-ZSM-5 from static and dynamic molecular simulations, ChemCatChem 6 (2014) 1906–1918.
[60] B.A. De Moor, M.-F. Reyniers, G.B. Marin, Physisorption and chemisorption of alkanes and alkenes in H-FAU: a combined ab initio-statistical thermodynamics study, Phys. Chem. Chem. Phys. 11 (2009) 2939–2958.
[61] G. Piccini, M. Alessio, J. Sauer, Y.C. Zhi, Y. Liu, R. Kolvenbach, A. Jentys, J.A. Lercher, Accurate adsorption thermodynamics of small alkanes in zeolites. ab initio theory and experiment for H-chabazite, J. Phys. Chem. C 119 (2015) 6128–6137.
[62] B.A. De Moor, A. Ghysels, M.F. Reyniers, V. Van Speybroeck, M. Waroquier, G.B. Marin, Normal mode analysis in zeolites: toward an efficient calculation of adsorption entropies, J. Chem. Theory Comput. 7 (2011) 1090–1101.
[63] G. Piccini, J. Sauer, Quantum chemical free energies: structure optimization and vibrational frequencies in normal modes, J. Chem. Theory Comput. 9 (2013) 5038–5045.
[64] G. Piccini, J. Sauer, Effect of anharmonicity on adsorption thermodynamics, J. Chem. Theory Comput. 10 (2014) 2479–2487.
[65] M. Piccini, Ab initio calculation of rate constants for molecule–surface reactions with chemical accuracy, Angew. Chem. Int. Ed. 55 (2016) 5235–5237.
[66] K. Alexopoulos, M.-S. Lee, Y. Liu, Y. Zhi, Y. Liu, M.-F. Reyniers, G.B. Marin, V.-A. Glezakou, R. Rousseau, J.A. Lercher, Anharmonicity and confinement in zeolites: structure, spectroscopy, and adsorption free energy of ethanol in H-ZSM-5, J. Phys. Chem. C 120 (2016) 7172–7182.
[67] C. Stegelmann, A. Andreasen, C.T. Campbell, Degree of rate control: how much the energies of intermediates and transition states control rates, J. Am. Chem. Soc. 131 (2009) 8077–8082.
[68] M. Choi, K. Na, J. Kim, Y. Sakamoto, O. Terasaki, R. Ryoo, Stable single-unit-cell nanosheets of zeolite MFI as active and long-lived catalysts, Nature 461 (2009) 246–U120.
[69] S. Svelle, P.O. Ronning, U. Olsbye, S. Kolboe, Kinetic studies of zeolite-catalyzed methylation reactions. Part 2. Co-reaction of [C-12]propene or [C-12]n-butene and [C-13]methanol, J. Catal. 234 (2005) 385–400.
[70] S. Svelle, P.A. Ronning, S. Kolboe, Kinetic studies of zeolite-catalyzed methylation reactions 1. Coreaction of [C-12]ethene and [C-13]methanol, J. Catal. 224 (2004) 115–123.